Device Simulation with Electromagnetic Field Propagation Models for High-Speed Image Sensors and FDA Noise Analysis

Hideki Mutoh
Link Research Corporation
291-4, Kuno, Odawara, Kanagawa, 250-0055 Japan
Phone: +81-465-34-6782, E-mail: hideki.mutoh@nifty.com

Abstract: **Physical models for device simulation for high-speed image sensors are proposed. To obtain consistent basic equations for both the device and electromagnetic field propagation simulations, we newly introduce a scalar field. The propagation of electromagnetic field induced by electrodes can be considered using the proposed equations and finite difference time domain (FDTD) method. Some characteristics of CMOS image sensors were calculated by this method. It is shown that floating diffusion amp (FDA) noise strongly depends on the substrate thickness.**

I. Introduction

Recently, the frame rate of high-speed image sensors has been drastically enhanced.[1-3] The device simulations of such devices are important to realize high sensitivity and high-speed perfect readout of signal charge from photodiodes.[4, 5] In near future, the device simulation with considering electromagnetic field propagation will be needed, because the propagation time of electric field induced by gate electrodes cannot be ignored in the future devices. But there is the serious problem that the basic equations for device simulations are not always consistent with Maxwell's equations to be satisfied by the model of electromagnetic field.

In general, the model of electromagnetic field is based on Maxwell's equations[9] written by

$$\mathbf{J} = \nabla\times\mathbf{H} - \varepsilon\frac{\partial\mathbf{E}}{\partial t}, \quad \rho = \varepsilon\nabla\mathbf{E}, \tag{1}$$

$$\nabla\times\mathbf{E} + \mu\frac{\partial\mathbf{H}}{\partial t} = 0, \quad \nabla\mathbf{H} = 0, \tag{2}$$

where ρ is charge density, $\mathbf{J}$ is current density, $\mathbf{H}$ is magnetic field vector, $\mathbf{E}$ is electric field vector. ε and μ are permittivity and permeability, which satisfy $\varepsilon\,\mu = 1/c^2$, where c denotes speed of light in the material. (1) gives the equation of charge conservation,

$$\nabla\mathbf{J} + \frac{\partial\rho}{\partial t} = 0. \tag{3}$$

On the other hand, device simulations are ordinarily based on Poisson's and current continuity equations[7, 8]

$$\varepsilon\nabla^2\psi = -q(N_D - N_A + p - n), \tag{4}$$

$$\nabla\mathbf{J}_p + q\frac{\partial p}{\partial t} = GR, \quad \nabla\mathbf{J}_n - q\frac{\partial n}{\partial t} = -GR, \tag{5}$$

where ψ is potential, p and n are hole and electron concentration , N_D and N_A are donor and acceptor ion concentration, $\mathbf{J}_p$ and $\mathbf{J}_n$ are hole and electron current density, q is magnitude of electronic charge, and GR is the carrier generation-recombination rate.

Since Maxwell's equations satisfy the principle of superposition,[9] holes and electrons must individually satisfy (1). Then,

$$\mathbf{J}_p = \nabla\times\mathbf{H}_p - \varepsilon\frac{\partial\mathbf{E}_p}{\partial t}, \quad \rho_p \equiv qp = \varepsilon\nabla\mathbf{E}_p, \tag{6}$$

where H_p and E_p are magnetic and electric fields induced by holes, respectively. Therefore, (5) is not satisfied in the case of $GR \neq 0$, because (6) gives

$$\nabla\mathbf{J}_p + \frac{\partial\rho_p}{\partial t} = 0. \tag{7}$$

Since the above situation is same for electrons, carrier generation and recombination are forbidden by Maxwell's equations. In addition to the above problem, electrode regions in device simulation do not satisfy the charge conservation. In silicon, current injection and absorption at electrode surfaces give $\nabla J \neq 0$ even in the steady state of $\partial\rho/\partial t = 0$. Gate electrodes also do not satisfy (3) in transient analysis, because gate surfaces give $\nabla J = 0$ and $\partial\rho/\partial t \neq 0$ when time dependent voltage is applied to the gate. Consequently, modification of Maxwell's equations is needed by the device simulation with considering electromagnetic field propagation to treat carrier generation-recombination and charge creation-annihilation at electrode surfaces.

II. Modification of Maxwell's equations

Using vector potential **A** and scalar potential ψ, electric field vector **E** and magnetic field vector **H** are written as

$$\mathbf{E} = -\nabla\psi - \frac{\partial \mathbf{A}}{\partial t}, \quad \mathbf{H} = \frac{1}{\mu}\nabla\times\mathbf{A}. \tag{8}$$

In order to realize current injection and absorption at electrode surfaces and carrier generation and recombination in semiconductor, we newly introduce the electromagnetic scalar field[6] γ defined by

$$\gamma = \nabla\mathbf{A} + \frac{1}{c^2}\frac{\partial\psi}{\partial t}. \tag{9}$$

In Lorenz gauge condition[9] of $\gamma = 0$, **J**, ρ, **A**, and ψ satisfy

$$\mu\mathbf{J} = -\Box\mathbf{A}, \quad \rho = -\varepsilon\Box\psi, \tag{10}$$

where $\Box$ is d'Alembertian defined by

$$\Box \equiv \nabla^2 - \frac{1}{c^2}\frac{\partial^2}{\partial t^2}. \tag{11}$$

If we assume (10) even in the case of $\gamma \neq 0$, current and charge density equations (1) is rewritten by

$$\mathbf{J} = \nabla\times\mathbf{H} - \varepsilon\frac{\partial\mathbf{E}}{\partial t} - \frac{1}{\mu}\nabla\gamma, \quad \rho = \varepsilon\nabla\mathbf{E} + \varepsilon\frac{\partial\gamma}{\partial t}. \tag{12}$$

Therefore, the carrier generation-recombination rate is given by

$$GR = \nabla\mathbf{J} + \frac{\partial\rho}{\partial t} = -\frac{1}{\mu}\Box\gamma. \tag{13}$$

The above relation permits current injection and absorption at electrode surfaces and carrier generation and recombination in semiconductor. It should be noticed that $GR = 0$ needs not $\gamma = 0$ but $\Box\gamma = 0$. Except the meaning of the scalar field γ, the above electromagnetic field model is equivalent to that of quantum electrodynamics (QED), which was proposed by E. Fermi[10, 11] at first and is known as the most accurate theory in physics now. The theoretical background of the above modification is also shown in Appendix.

III. Device simulations considering electric field propagation

It is difficult to consider the propagation of magnetic field induced by gate electrodes, because of complexity of current calculation in gate electrodes. If we consider only electric and scalar fields, the simulation of the field propagation is much simpler than the above case, by assuming

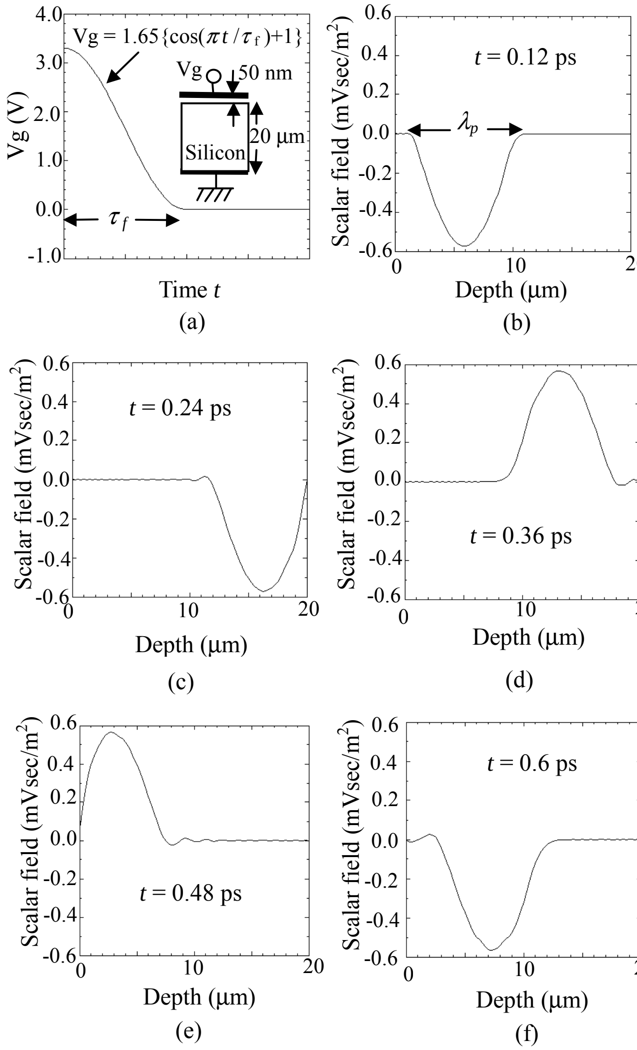

Fig. 1. 1D simulation result of scalar field distribution dependence on time. λ_p denotes the wave packet length. (a) Vg dependence on time (τ_f = 0.1 ps) and the analyzed structure. The scalar field along depth direction is shown in (b) t = 0.12 ps, (c) t = 0.24 ps, (d) t = 0.36 ps, (e) t = 0.48 ps, and (f) t = 0.6 ps.

$$|\nabla\times\mathbf{H}| << \left|\varepsilon\frac{\partial\mathbf{E}}{\partial t} + \frac{1}{\mu}\nabla\gamma\right|. \tag{14}$$

Then, electromagnetic field propagation in semiconductor can be calculated by considering only electric and scalar fields. The discritization of the fields can be done by FDTD method.[6, 12] The following analyses were performed by assuming $\nabla\mathbf{A} = 0$.

A. 1D field propagation analysis

The analyzed structure and the gate pulse shape are shown in Fig. 1 (a), where τ_f denotes the fall time of driving pulse. Fig 1 (b)-(f) show the scalar filed distribution along depth direction at t of 0.12, 0.24, 0.36, 0.48, and 0.6 ps in the case of τ_f = 0.1 ps. The sign of the scalar field is changed by every reflection at the gate and substrate electrodes.

Since the absorption coefficient is very small for the wavelength more than 1 µm, the scalar field wave packet induced by gate electrode driving pulse exists in the silicon substrate for long time, by multi-reflection of the gate and substrate electrodes. Since the wave packet length λ_p is given by $c\tau_f$, τ_f of 0.1 ps gives λ_p of 9 µm in silicon and 30 µm in vacuum.

B. Readout potential analysis

Fig. 2 (a) shows the 2D analyzed structure of CMOS image sensor including a photodiode, a transfer gate, and a floating diffusion. The transfer gate voltage is linearly changed from 0 to 3.3 V by the driving pulse with rise time τ_r as shown in Fig. 2 (b). The potential distribution with τ_r of 0.1 ps at t = 0, 0.2, 0.85, and 1.0 ps are shown in Fig. 2 (c), (d), (e), and (f), respectively. Although the potential well of photodiode region is collapsed at t = 0.2 ps, it is recovered at t = 0.85 ps.

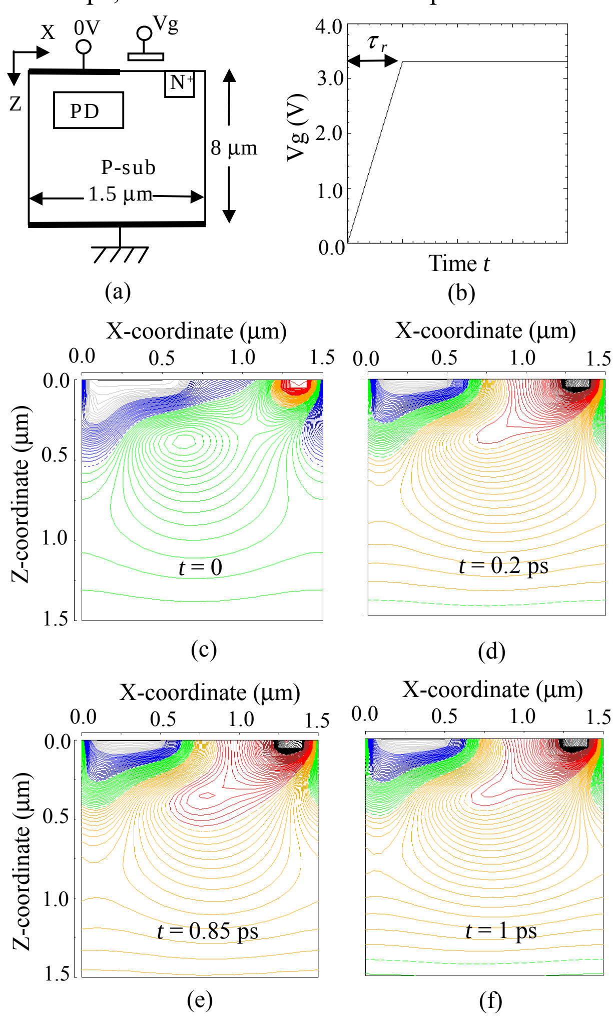

Fig. 2. CMOS image sensor potential distribution dependence on time (τ_r = 0.1 ps). (a) Analyzed structure. (b) Vg dependence on time. (c) t = 0. (d) t = 0.2 ps. (e) t = 0.85 ps. (f) t = 1 ps.

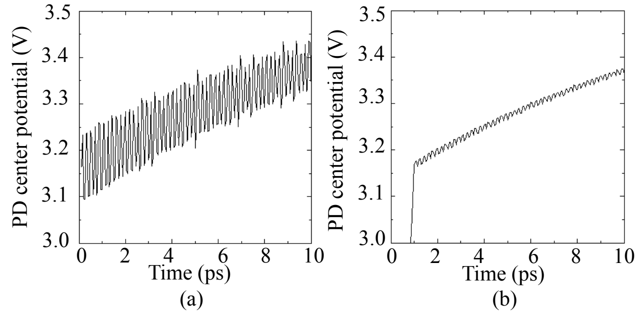

Fig. 3. Photodiode (PD) center potential dependence on time (x = 0.8, z =0.35). (a) τ_r = 0.1 ps. (b) τ_r = 1 ps.

This potential vibration seems to be caused by the multi-reflected wave packet in silicon substrate induced by the transfer gate driving pulse. Fig. 3 shows the potential dependence on time at the center of the photodiode in the case of τ_r = 0.1 ps (a) and τ_r = 1 ps (b). The amplitude of the potential vibration of τ_r = 0.1 ps is much larger than that of τ_r = 1 ps.

C. FDA noise analysis

Fig. 4 (a) shows the 2D structure including a floating diffusion and a transfer gate. The potential vibration amplitude dependence on the

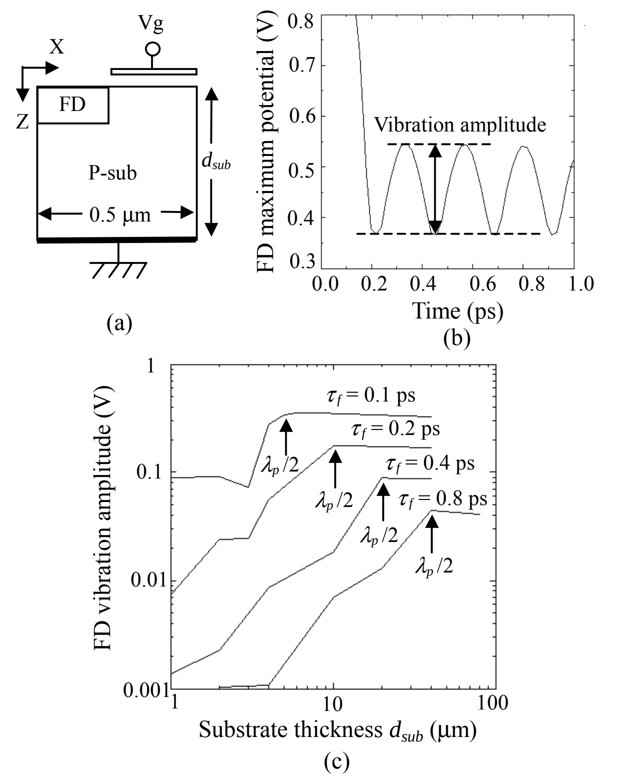

Fig. 4. Floating diffusion (FD) potential vibration dependence on time, where Vg is same as Fig. 1 (a). (a) Analyzed structure. (b) FD maximum potential dependence on time for τ_f = 0.2 ps and d_{sub} = 10 µm. (c) FD potential vibration amplitude dependence on the fall time τ_f and substrate thickness d_{sub}, where λ_p is the wave packet length as shown in Fig. 1 (b).

fall time τ_f of the transfer gate driving pulse and the substrate thickness d_{sub} is calculated. The driving pulse shape is same as Fig. 1 (a). Fig. 4 (b) shows the maximum potential dependence on time in the floating diffusion for τ_f = 0.2 ps and d_{sub} = 10 μm. Fig. 4 (c) shows the potential vibration amplitude dependence on the fall time and the substrate thickness. The shorter fall time results the larger vibration amplitude, which is steeply decreases with reduction of the substrate thickness in the case of $d_{sub} < \lambda_p/2$, although it is nearly constant in the case of $d_{sub} \geq \lambda_p/2$, where λ_p denotes the wave packet length as shown in Fig. 1 (b). This is explained by the interference between top and tail of the wave packet. It seems that the FDA noise caused by the driving pulses can be reduced by decreasing the substrate thickness. The interference of electromagnetic wave packet might be the reason why the noise of a backside illuminated image sensor is reduced by thinning the substrate.

IV. Conclusion

The novel device simulation method with electromagnetic field propagation models including the scalar field was proposed. It can analyze the readout characteristics of ultra-high speed image sensors and noise characteristics of FDA. It was found that the FDA noise induced by driving pulses might be reduced by controlling the substrate thickness.

References

1) T. G. Etoh, et al.: “An image sensor which captures 100 consecutive frames at 1000000 frames/s,” *IEEE Trans. Electron Devices*, **50**, pp. 144-151, 2003.
2) T. G. Etoh, et al.: “A 16 Mfps 165kpixel backside-illuminated CCD,” *ISSCC 2011 Dig. Tech. Papers*, pp. 406-408, 2011.
3) Y. Tochigi, et al.: “A Global-Shutter CMOS Image Sensor with Readout Speed of 1 Tpixel/s Burst and 780Mpixel/s Continuous,” *IEEE J. Solid-State Circuits,* **48**, no. 1, pp. 329-338, 2013.
4) H. Mutoh: “Simulation for 3-dimensional optical and electrical analysis of CCD,” *IEEE Trans. Electron Devices*, **44,** pp. 1604-1610, 1997.
5) H. Mutoh: "3-D Optical and Electrical Simulation for CMOS Image Sensors,” *IEEE Trans. Electron Devices*, **50,** pp. 19-25, 2003.
6) H. Mutoh: “Physical Models and Algorithms for Device Simulation for High-Speed Image Sensors,” *J. Institute of Image Information and Television Engineers*, **67**, no.3, pp. J89-J94, 2013. [Available online]: https://www.jstage.jst.go.jp/article/itej/67/3/67_J89/_pdf
7) S. M. Sze: *Physics of Semiconductor Devices*, Wiley, New York, 2nd ed., pp. 50-51, 1981.
8) S. Selberherr: *Analysis and Simulation of Semiconductor Devices*, Springer, Wien, pp. 8-11, 1984.
9) R. P. Feynman, R. B. Leighton, and M. L. Sands: *Feynman Lectures on Physics*, **2**, Addison-Wesley, Massachusetts, 1965.
10) E. Fermi: “Quantum Theory of Radiation,” *Rev. Mod. Phys*. **4**, pp. 87-132, 1932.
11) S. S. Schweber: *An Introduction to Relativistic Quantum Field Theory*, (Harper & Row, New York, 1962), Chap. 9, p. 242, 1962.
12) A. Traflove: *Computational Electrodynamics: The Finite-Difference Time-Domain Method*, Artech House, Norwood, MA, 1995.

Appendix

Maxwell’s equations (1) and (2) can be written as follows, using a complex field, $\mu\mathbf{H}+i\mathbf{E}/c$.

$$\mu\begin{pmatrix} J_x \\ J_y \\ J_z \\ ic\rho \end{pmatrix} = \begin{pmatrix} i\partial_{ct} & -\partial_z & \partial_y \\ \partial_z & i\partial_{ct} & -\partial_x \\ -\partial_y & \partial_x & i\partial_{ct} \\ \partial_x & \partial_y & \partial_z \end{pmatrix} \begin{pmatrix} \mu H_x + iE_x/c \\ \mu H_y + iE_y/c \\ \mu H_z + iE_z/c \end{pmatrix}, \qquad \text{(A1)}$$

where

$$\partial_x \equiv \frac{\partial}{\partial x},\ \partial_y \equiv \frac{\partial}{\partial y},\ \partial_z \equiv \frac{\partial}{\partial z},\ \partial_{ct} \equiv \frac{\partial}{c\partial t}. \qquad \text{(A2)}$$

The relation between the field and the potential can be written by

$$\begin{pmatrix} \mu H_x + iE_x/c \\ \mu H_y + iE_y/c \\ \mu H_z + iE_z/c \end{pmatrix} = \begin{pmatrix} -i\partial_{ct} & -\partial_z & \partial_y & -\partial_x \\ \partial_z & -i\partial_{ct} & -\partial_x & -\partial_y \\ -\partial_y & \partial_x & -i\partial_{ct} & -\partial_z \end{pmatrix} \begin{pmatrix} A_x \\ A_y \\ A_z \\ i\psi/c \end{pmatrix}. \qquad \text{(A3)}$$

Since current and potentials are 4-dimensional parameters, the complex field should be extended to 4-dimension. Then (A1) and (A3) are naturally extended as follows, using a scalar filed γ,

$$\mu\begin{pmatrix} J_x \\ J_y \\ J_z \\ ic\rho \end{pmatrix} = \begin{pmatrix} i\partial_{ct} & -\partial_z & \partial_y & -\partial_x \\ \partial_z & i\partial_{ct} & -\partial_x & -\partial_y \\ -\partial_y & \partial_x & i\partial_{ct} & -\partial_z \\ \partial_x & \partial_y & \partial_z & i\partial_{ct} \end{pmatrix} \begin{pmatrix} \mu H_x + iE_x/c \\ \mu H_y + iE_y/c \\ \mu H_z + iE_z/c \\ \gamma \end{pmatrix}, \qquad \text{(A4)}$$

$$\begin{pmatrix} \mu H_x + iE_x/c \\ \mu H_y + iE_y/c \\ \mu H_z + iE_z/c \\ \gamma \end{pmatrix} = \begin{pmatrix} -i\partial_{ct} & -\partial_z & \partial_y & -\partial_x \\ \partial_z & -i\partial_{ct} & -\partial_x & -\partial_y \\ -\partial_y & \partial_x & -i\partial_{ct} & -\partial_z \\ \partial_x & \partial_y & \partial_z & -i\partial_{ct} \end{pmatrix} \begin{pmatrix} A_x \\ A_y \\ A_z \\ i\psi/c \end{pmatrix}. \qquad \text{(A5)}$$

(A4) and (A5) give (2), (8), (9), (10), (12), and (13). Then $-\mathbf{JE}+c^2\rho\gamma$ is written by

$$-\mathbf{JE} + c^2\rho\gamma = \nabla\left(\mathbf{E}\times\mathbf{H} + \frac{\gamma\mathbf{E}}{\mu}\right) + \frac{\partial}{\partial t}\left(\frac{\varepsilon E^2}{2} + \frac{\mu H^2}{2} + \frac{\gamma^2}{2\mu}\right). \qquad \text{(A6)}$$

Since the above equation is regarded as the continuity equation for energy density, $-\mathbf{JE}+c^2\rho\gamma$ is energy generation rate, $\mathbf{E}\times\mathbf{H}+\gamma\mathbf{E}/\mu$ is the energy flow vector, and $(\varepsilon E^2+\mu H^2+\gamma^2/\mu)/2$ is the energy density. The additional term of the energy density $\gamma^2/(2\mu)$ suggests that electromagnetic field energy density is increased by existence of the scalar field.